Weather and Climate Extremes 48 (2025) 100748

Contents lists available at ScienceDirect

Weather and Climate Extremes

journal homepage: www.elsevier.com/locate/wace

Regional drivers and characteristics of multi-year droughts

Jonna van Mourik [a,*], Denise Ruijsch [a], Karin van der Wiel [a,b], Wilco Hazeleger [a], Niko Wanders [a]

[a] Department of Physical Geography, Faculty of Geosciences, Utrecht University, Utrecht, The Netherlands
[b] Royal Netherlands Meteorological Institute (KNMI), De Bilt, The Netherlands

ARTICLE INFO

Dataset link: https://doi.org/10.24416/UU01-MQT1NN

Keywords:
Multi-year droughts
SPEI-12
Precipitation
Potential evapotranspiration
Predictability

ABSTRACT

Multi-year droughts (MYDs) are severe natural hazards that have become more common due to climate change. Given their significant societal impact compared to droughts of shorter duration, it is crucial to better understand the drivers of MYDs. Using reanalysis data, this study provides a historical overview of MYDs in California, Western Europe, India, central Argentina, South Africa, and southeast Australia. For each region, the characteristics and drivers of the multi-year droughts are given and compared to those of normal droughts (NDs). Additionally, we investigated the potential for longer-term memory of droughts. Our findings reveal that MYD occurrence and duration vary significantly per region, with relatively larger differences in duration between MYDs and NDs observed in California, Argentina, and Australia. Regions with distinctive seasonality in their precipitation climatology tend to experience faster drought onsets compared to regions with climatologically steady precipitation. Our analysis shows that MYDs and NDs often start with similar conditions but diverge over time, with larger potential evapotranspiration values for most regions, and additional lower precipitation rates for Argentina and India. Longer-term memory is present in Argentina, Australia, and South Africa, which might provide avenues for the predictability of MYDs in these regions. Teleconnections influenced by oceans and land are expected to play a significant role here, while in other regions MYD occurrence may be more subject to chance. These findings can aid in decision-making on water management, preceding and during droughts.

1. Introduction

Recent decades have been marked by extended periods of severe drought worldwide. Australia, for example, faced the Millennium drought from 2001 to 2009, which was described as the worst drought in the instrumental record for southeastern Australia (Van Dijk et al., 2013). After an eight-year break, it was followed by another period of below-average rainfall, lasting from 2017 to 2020 (King et al., 2020). In South Africa, Cape Town nearly exhausted its water supply in 2018 due to a multi-year drought (Otto et al., 2018; Burls et al., 2019; Pascale et al., 2020). From 2019 to 2022 Argentina experienced a drought which was unprecedented in the last 50 years (Rivera, 2024). In Europe, the succession of dry summers following the 2018 summer drought showed that long-lasting droughts are not limited to arid and semi-arid regions (Rakovec et al., 2022). Because these droughts have hydrological consequences lasting several years, they are called multi-year droughts (MYDs). While not a new phenomenon in the historical record, they are occurring increasingly over all continents, which is attributed to anthropogenic climate change (Wu et al., 2022).

The multi-year nature of these droughts has implications for water management (Kreibich et al., 2022), groundwater availability, and increased crop vulnerability (Lesk et al., 2022). Because of these consequences, it is important to understand the characteristics of multi-year droughts and the drivers that initiate and prolong them. Many studies focus on aspects of individual MYD events. For example, Luo et al. (2017) demonstrated that the 2012–2015 multi-year drought in California was initiated by a winter high pressure ridge off the West Coast of North America, and was sustained by subsequent high pressure ridges in the following winters. For the MYD in Europe that started in 2018, Dirmeyer et al. (2021) found that low soil water limited surface latent heat fluxes, resulting in a land-atmosphere feedback that exacerbated the drought during the summer of 2018. However, Van der Wiel et al. (2023) found no evidence for multi-year (i.e. from summer 2018 to summer 2019) meteorological drivers here. Other studies focused on the effect of anthropogenic climate change on the likelihood of occurrence of MYDs (e.g. Pascale et al., 2021; Van der Wiel et al., 2023), or modelled how such droughts might manifest in a future climate (Gupta and Jain, 2018; Gessner et al., 2022). Additionally, some studies focus on multiple MYDs that occurred in the same area in order to compare their meteorological conditions (e.g. Parry et al., 2012). Often, studies examine the first year of a drought only and not

* Corresponding author.
E-mail address: j.vanmourik1@uu.nl (J. van Mourik).

https://doi.org/10.1016/j.wace.2025.100748
Received 19 September 2024; Received in revised form 10 December 2024; Accepted 11 February 2025
Available online 21 February 2025

Table 1
Overview of reanalysis and observational data used in this study. All reanalysis data is time-averaged to daily values, and the observational data to monthly values. Everything is regridded to 0.5° × 0.5°, except for GPCP due to its lower resolution.

Dataset	Time period	Time step	Resolution	References
Reanalysis				
ERA-5	1950–2023	Hourly	0.25° × 0.25°	Hersbach et al. (2023)
MERRA-2	1980–2023	Hourly	0.5° × 0.625°	Gelaro et al. (2017)
JRA-3Q	1951–2023	Six-hourly	0.375° × 0.375°	Japan Meteorological Agency (2023)
Observations				
CHIRPS	1981–2023	Monthly	0.25° × 0.25°	Funk et al. (2015)
CRU TS 4.03	1941–2018	Monthly	0.5° × 0.5°	University of East Anglia Climatic Research Unit Jones and Harris (2008)
E-OBS 29.0e	1950–2023	Daily	0.25° × 0.25°	Cornes et al. (2018)
GPCP	1979–2023	Monthly	2.5° × 2.5°	Adler et al. (2018)
IMERG	2000–2023	Monthly	0.1∘ × 0.1°	Huffman et al. (2023)

its full duration (Benedict et al., 2021) or do not distinguish between long and short droughts (Mishra et al., 2019). Concluding, neither the drivers of MYDs nor the differences between short and long-duration droughts have been systematically studied at global scale.

In general, knowledge of individual multi-year droughts is present, but there is no shared view among scientists and water managers. One of the problems is the lack of a commonly accepted definition for multi-year droughts. This is partly due to the variety of drought indices that are being used (Mukherjee et al., 2018; Han and Singh, 2023), combined with the absence of consensus on the minimum duration of a multi-year drought. For instance, Brunner and Tallaksen (2019) defines multi-year droughts to last longer than a year, whereas Wu et al. (2022) considers only those that persist for more than five years. These differences in definition make it challenging to compare different studies, as the lack of consensus results in no clear distinction between multi-year droughts and shorter 'normal' droughts (NDs). Nonetheless, knowing whether a region experiences a 'normal' or a multi-year drought is vital for decision-making in water management, as they require different strategies to mitigate their respective impact (Bachmair et al., 2016).

The objective of this study is to analyse the differences between 'normal' and multi-year droughts, along with their respective drivers, to identify potential early indicators for multi-year droughts during or preceding a drought. This comparison aims to determine whether multi-year droughts are fundamentally different phenomena or simply extreme right-tail outliers in the drought duration distribution. We will focus on six different regions around the world, with different climatological and hydrological properties. This will create a representative overview of when and where multi-year droughts occur, their key characteristics, and what sets them apart from 'normal' droughts, using reanalysis and observational data. These six focus regions will serve as examples but will not cover all MYD possibilities. However, our method can be applied to any region of interest. Historic overviews and characterization of typical events like these are important for assessing the capability of climate models to accurately reproduce multi-year droughts, their drivers and spatial–temporal characteristics for different climate regions. Finally, we will investigate the potential role of long-term drivers, such as ocean and land anomalies influencing the weather via teleconnections, in the duration of droughts, aiming to assess if and where long-term predictability of multi-year droughts might be possible.

2. Methods

2.1. Data

In this study, we used data from the ERA5 reanalysis dataset, which provides data with a spatial resolution of 0.25° × 0.25° and an hourly temporal resolution (Hersbach et al., 2023). To characterize MYDs, we used the following variables from this dataset: total precipitation (PR), 2 m temperature ($t2m$), 2 m dewpoint temperature ($d2m$), sea level pressure (slp), 10 m zonal component of wind ($u10$), 10 m meridional component of wind ($v10$), surface net solar radiation (ssr) and surface net thermal radiation (str) for the period 1950–2023. Because of the large spatial scale of MYDs and to reduce computational demand, all variables were regridded to 0.5° × 0.5°. Additionally, since this study covers timescales of multiple years and drought is a slow-developing phenomenon, the temporal resolution was upscaled from an hourly to a daily resolution. For all meteorological variables, daily mean or accumulated values were calculated, just as the daily minimum and maximum values for the 2 m temperature and 2 m dewpoint temperature.

While the ERA5 reanalysis dataset is widely regarded as a state-of-the-art product and serves as the baseline for this study, we evaluated the robustness of our results by comparing results based on ERA5 to other reanalyses and observational datasets (Table 1). Results of this analysis can be found in the Supplementary Information (SI) (Sections S.3 and S.4).

2.2. Multi-year drought definition

To quantify MYDs we applied the 12-month averaged Standardised Precipitation-Evapotranspiration Index (SPEI-12, Vicente-Serrano et al., 2010), a commonly used drought indicator to characterize hydrological droughts. It has the advantage of including a broad spectrum of global meteorological data and does not solely rely on local precipitation measurements. The SPEI-12 calculation itself is done using the Python Package of $xclim$ (Bourgault et al., 2023). SPEI follows from the water balance, consisting of the standardized difference between precipitation (PR) and potential evapotranspiration (PET, Thornthwaite, 1948):

$$D_i = PR_i - PET_i, \tag{2.1}$$

where D_i is the difference between the precipitation PR_i and the potential evapotranspiration PET_i per month i. For the calculation of SPEI-12 for one study region, the precipitation and potential evaporation are first averaged over all gridcells within the study region, before calculating the water balance. The water balance is normalized after aggregating over a 12-month timescale. This D_i timeseries is fitted using a three-parameter log–logistic probability function, which leads to SPEI-12 timeseries per study region. Further explanation can be found in Appendix B.

The potential evaporation is calculated using the Penman-Monteith (FAO56) method from the $pyet$ package (Vremec et al., 2023; Penman, 1948; Monteith, 1965), in which the near-surface air temperature ($t2m$), dewpoint temperature ($d2m$), surface pressure (sp), horizontal wind velocity ($u10$, $v10$), surface net solar radiation (ssr), and surface net thermal radiation (str) are included. Combined they appear in the following equation where the potential evapotranspiration is calculated:

$$PET = \frac{0.408\Delta(R_n - G) + \gamma \frac{900}{T+273} u_2 (e_s - e_a)}{\Delta + \gamma(1 + 0.34u_2)}. \tag{2.2}$$

In this equation, the soil heat flux density (G) is assumed to have a daily average of zero. All other variables are provided in Table 2, which also includes information on how these variables were derived from the ERA5 archive, and further information on the formulas involved

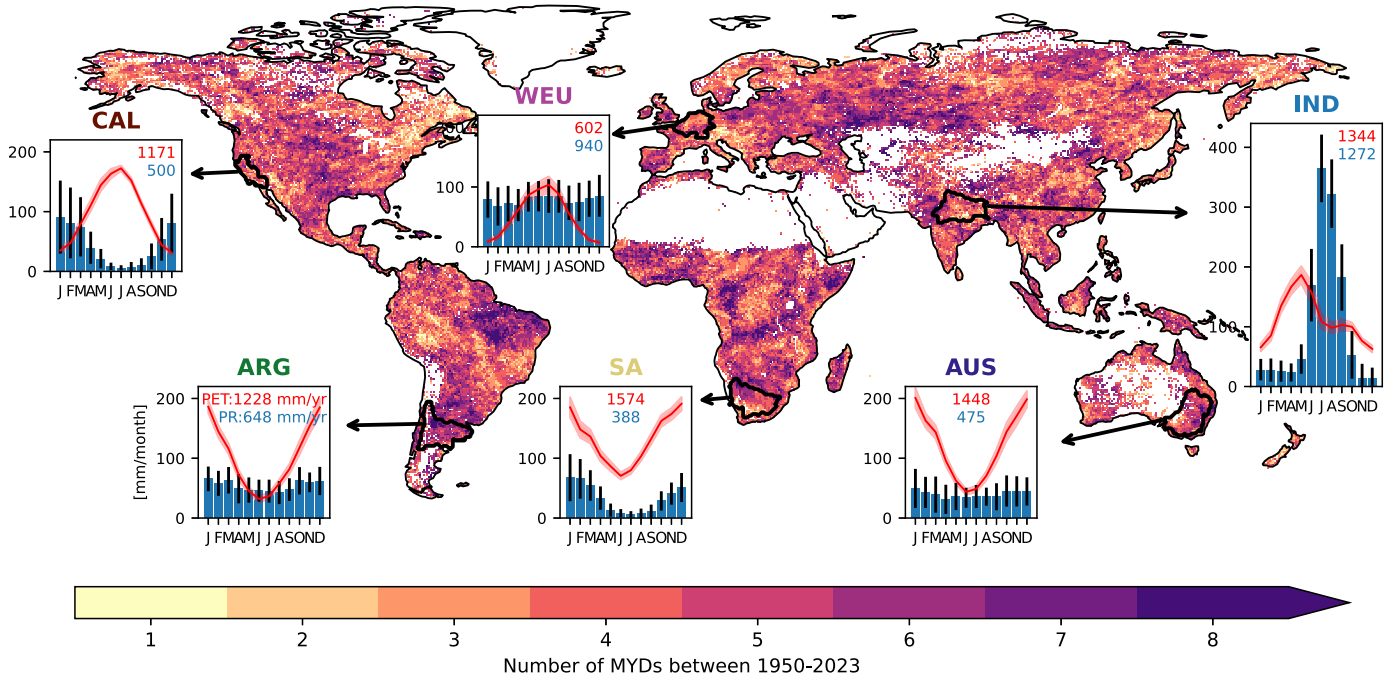

Fig. 1. Map of the number of Multi-Year Droughts (MYDs). Focus regions are chosen to represent different continents and climates (see Section 2.3), and are denoted by a black lining. For each focus region, the monthly climatology of precipitation (PR, [mm/month], blue bars) and potential evaporation (PET, [mm/month], red line) is shown, including one standard deviation from the mean with small bars for precipitation and shading for PET. In the upper right corner of each region, the total amount of precipitation and PET per year is shown. Regions with sparse vegetation or with permanent snow and ice are masked and shown in white. (For interpretation of the references to colour in this figure legend, the reader is referred to the web version of this article.)

Table 2
Variables included in Eq. (B.4) (first column), their meaning and units (second and third column), and which ERA5 variables were needed to derive them (last column).

Variable	Meaning	Unit	Calculated from
PET	Reference evapotranspiration	mm day^{-1}	All variables
R_n	Net radiation at the crop surface	MJ m^{-2} day^{-1}	ssr, str
G	Soil heat flux density	MJ m^{-2} day^{-1}	Assumed 0
T	Mean daily air temperature at 2 m height	°C	$t2m$
u_2	Wind speed at 2 m height	m s^{-1}	$u10$, $v10$
e_s	Saturation vapour pressure	kPa	$t2m$
e_a	Actual vapour pressure	kPa	$d2m$
Δ	Slope vapour pressure curve	kPa °C^{-1}	$t2m$
γ	Psychometric constant	kPa °C^{-1}	sp

can be found in Appendix B. A further comparison with a simpler PET calculation based on solely radiation can be found in SI Section S.5.

From the SPEI-12 timeseries we identified the initiation and termination of MYD events using the 'run theory' of Yevjevich et al. (1967), which defines a drought as a consecutive period below a certain threshold of a drought index. As a threshold, we chose the value of SPEI-12 ≤ -1, which represents the 16% driest months of the SPEI-12 timeseries (Um et al., 2017; García-Valdecasas Ojeda et al., 2021). For classification as a multi-year drought, we required SPEI-12 ≤ -1 to persist for at least 12 consecutive months (Van der Wiel et al., 2023). Since the SPEI-12 already incorporates the 12 months prior in its running mean, a year of SPEI-12 ≤ -1 indicates that weather conditions leading to the MYD were established in the preceding year. The number of MYDs in the ERA5 record (1950–2023) following from this method are shown in Fig. 1.

2.3. Study regions

We applied our analysis to a selection of study regions spread over the continents, characterized by their climate and geographical location. To test the validity of our method and to have a broad spectrum of multi-year drought characteristics, we aimed for these regions to be representative of different climates, but also adhere to a few requirements. To start, each region should have experienced past high-impact MYDs, but they do not necessarily have to be the region with the highest number of MYDs on a continent. Moreover, we prioritized regions that are inhabited or used for food production, ensuring relevance to communities affected by drought impacts. Next to these demographic and drought conditions, we also required our regions to conform to the natural boundaries of river basins. This allows us to study the water balance of these regions, as precipitation and evapotranspiration are balanced by water storage change and discharge from the land surface into the ocean. Furthermore, the size of selected regions needed to approximate the spatial scale of dominating weather systems, to increase the chances of the whole region experiencing drought at the same time. To verify this, we conducted a correlation and a semi-variogram analysis to find the typical spatial impact region of the geopotential height field at 500 hPa. This analysis is further discussed in SI Section S.2.

Using these requirements, we selected the following study regions (Fig. 1): California (CAL), the Rhine-Meuse delta in Western Europe (WEU), the Ganges delta in India (IND), central Argentina (ARG), the Orange River basin in South Africa (SA), and the Murray-Darling basin in Australia (AUS). India, South Africa, and Australia have individual

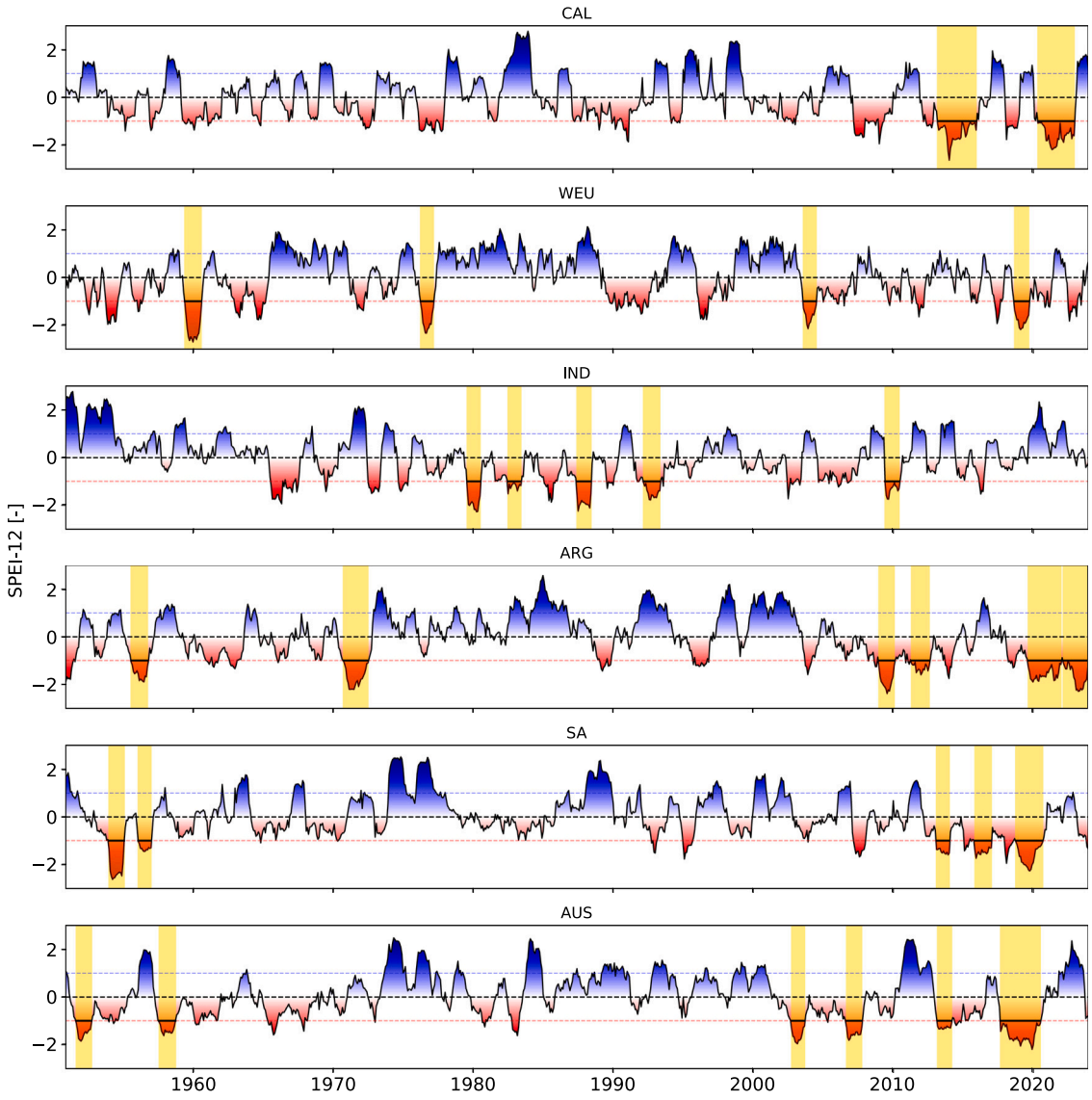

Fig. 2. SPEI-12 [-] timeseries from 1950–2023 for all six focus regions. Values above zero indicate wet periods (blue), and values below zero indicate dry periods (red). MYDs are marked by a horizontal black line at SPEI-12 = −1 and a yellow background between the start and end dates of the events. Additional horizontal lines are drawn at SPEI-12 = −1 (red, dotted), and SPEI-12 = 1 (blue, dotted) for better visibility of anomalous dry and wet periods. Figure made using the package of Vonk (2022) as a basis. (For interpretation of the references to colour in this figure legend, the reader is referred to the web version of this article.)

basins, while the others comprise multiple hydrological basins. California and India were chosen as their MYDs occur in different periods of time. For California, the MYDs occur in the 21st century, while almost all MYDs in India occurred in the 20th century. The basins of Western Europe, South Africa, and Argentina were chosen because of their recent exposure to severe MYDs (Rivera et al., 2021; Rakovec et al., 2022; Burls et al., 2019). Lastly, Australia was chosen because of its substantial amount of MYDs from 1950 onwards, including the Millennium drought.

For all these regions, the PET and precipitation climatologies are plotted in Fig. 1. It is clear that these represent various climate regimes. Western Europe, Argentina, and Australia have comparable precipitation and PET climatologies, where precipitation is constant throughout the year, although in different absolute quantities per region. Potential evapotranspiration has its peak in their respective summer and declines in winter. Any month with decreased precipitation can therefore result in a drought, although the probabilities of enhancement of the drought are higher in local summer due to higher PET values. The absolute PET values are also higher for Argentina and Australia than they are for Western Europe. California, South Africa and India all have a distinct seasonality with alternating wet and dry periods. For these three regions, reduced precipitation in the wet season means missing a significant water source for the rest of the year. California has wet winters and dry summers coinciding with high atmospheric water demands during summer. The rain that falls in winter is also highly variable and is dependent on atmospheric rivers, which are responsible for 20–50% of the state's precipitation (Dettinger et al., 2011). South Africa has its wet season during austral summer, and it depends on this precipitation for the rest of the year. The wet season coincides with large atmospheric water demands, although these values are still high in winter. India experiences completely different climatic circumstances, as it depends on the monsoons for its precipitation. This leads to just a few months of intense rainfall, preceded by a period of high atmospheric water demand. Most monsoons will compensate for the high demand, but a delayed or diminished monsoon can lead to a year of drought.

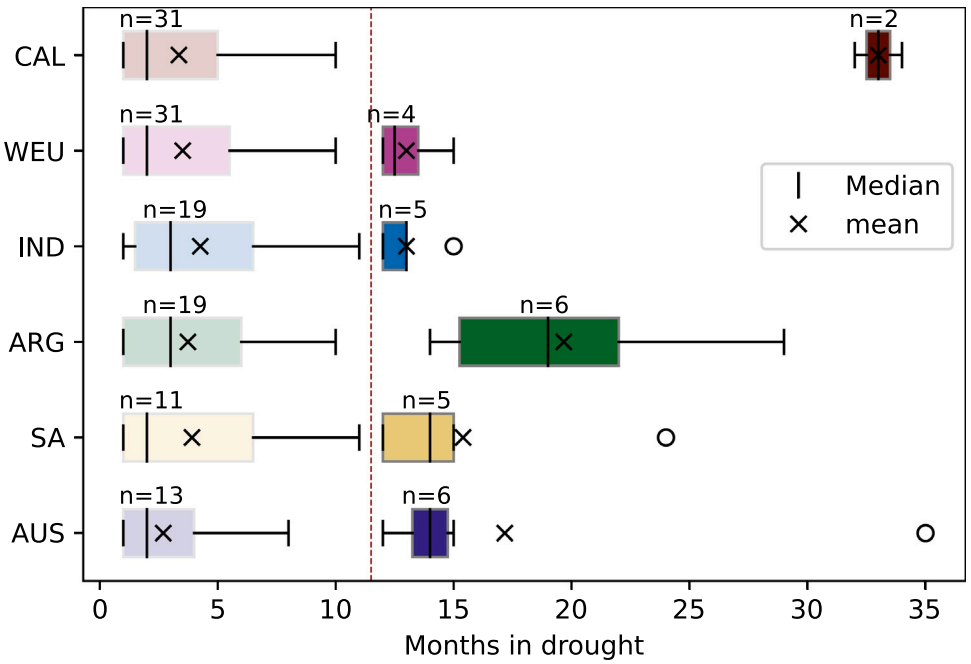

Fig. 3. Boxplot with drought durations for NDs (lighter coloured) and MYDs (darker coloured), separated by a vertical line at $x = 11.5$. The box indicates the first (Q1) and third (Q3) quartiles. Whiskers are placed at the minimum and maximum values within 1.5 times the interquartile range (IQR). The outliers outside of this range are indicated by open circles. The median (vertical shirt line within the box) and mean (cross) of the durations are also shown. (For interpretation of the references to colour in this figure legend, the reader is referred to the web version of this article.)

3. Results

3.1. Statistics on MYDs

In this section, we characterize MYDs in the six focus regions. For these regions, SPEI-12 timeseries indicating wet and dry periods are shown in Fig. 2, with MYD events marked. The exact dates at which the MYDs start and end are shown in Table A.1, together with their duration. To ensure that the MYD index represents experienced drought events, we compared the obtained MYD data to the literature and included relevant papers in this table. In terms of the amount of MYDs over the ERA5 period (1950–2023), the lowest number is found for California with only two events, both occurred after 2010. In contrast, Argentina and Australia each had six MYDs. However, the last two MYDs of Argentina occurred within one month of each other, it could therefore be argued this was a single MYD. With four MYDs for Western Europe and five for India and South Africa, these regions are on the intermediate to high side. The differences between these regions are not caused by the drought index, which per definition has the same mean and standard deviation wherever applied, but are caused by different drought dynamics, which we aim to characterize in this paper.

There are also differences in the temporal recurrence of MYDs between the regions. While MYDs seem to occur somewhat regularly every 14–26 years in Western Europe, all other regions show a higher degree of clustering of multiple events. Especially the regions in the southern hemisphere had a period between the late 1970s and early 2000s where no MYDs occurred at all, while at the same time, many MYDs developed in India. Conversely, India experienced a relatively wet period after 2010, while all other regions suffered from one (WEU) or more (CAL, ARG, SA, and AUS) MYDs. Besides these differences, there are also some commonalities in the MYD timeseries. Generally, the droughts that we have identified as MYDs using our MYD index are also the droughts with the lowest SPEI-12 values, going well below the −1 threshold. Exceptions are the droughts in California in 2008 and India in 1965, where the SPEI-12 timeseries briefly rises above −1 before reaching a 12-month period.

Looking at the occurrence of NDs compared to MYDs we observe that every region experienced more NDs than MYDs, although the exact ratio varies (Fig. 3). In California, only 6% of all droughts are MYDs, while in South Africa and Australia respectively 31% and 32% of all droughts are MYDs. California and Argentina stand out as their MYDs have the longest mean (μ) and medium (m) durations: $\mu = m = 33$ months for California; $\mu = 20$ and $m = 19$ months for Argentina. South Africa and Australia have individual MYDs with long durations of 24 and 35 months, respectively, but on average MYDs last 14 months for both. From the distance between the boxes for the NDs and the MYDs, we estimate that for Western Europe, India, and South Africa these MYDs are most likely the most extreme (right-tail) events of a single drought duration distribution. For California, Argentina, and Australia there is a clear separation between (some) MYDs and NDs and thus we hypothesize that for these long MYDs different physical processes are at play leading to the longer duration compared to the shorter NDs.

Besides the total number of NDs and MYDs, the total months that these regions experience both types of droughts is also of interest as they give a better indication of their relative drought impact (Table 3). Western Europe spends the least absolute amount of time in MYDs, with only 52 months in the total record, while Argentina has more than double that time in MYD with 118 months. Conversely, the shortest total drought duration of NDs is found for Australia, while the longest occurs in Western Europe. In Western Europe MYDs make up only 5.9% of the total timeseries, while NDs constitute 12.4%. Notably, all three regions in the northern hemisphere show fewer months in MYDs than in NDs, contrary to the southern hemisphere. Especially Australia has a high percentage of months in MYDs, reaching 11.8%. Australia timeries thus show almost three times as much time in MYDs as in NDs (4.0%), even though the absolute number of MYDs is lower than the number of NDs. Possible explanations for this distinction between these regions will be discussed in Section 3.4.

3.2. Temporal development of MYDs

What cannot be deduced from Fig. 2, is how long it takes for a meteorological drought to propagate into a multi-year hydrological drought,

Table 3
Percentages (months) in drought per region. Total months in the ERA5 record is 876 months.

	CAL	WEU	IND	ARG	SA	AUS
ND	11.9% (104)	12.4% (109)	9.2% (81)	8.2% (72)	4.9% (43)	4.0% (35)
MYD	7.5% (66)	5.9% (52)	7.4% (65)	13.5% (118)	8.8% (77)	11.8% (103)
Total drought	19.4% (170)	18.4% (161)	16.7% (146)	21.7% (190)	13.7% (120)	15.8% (138)

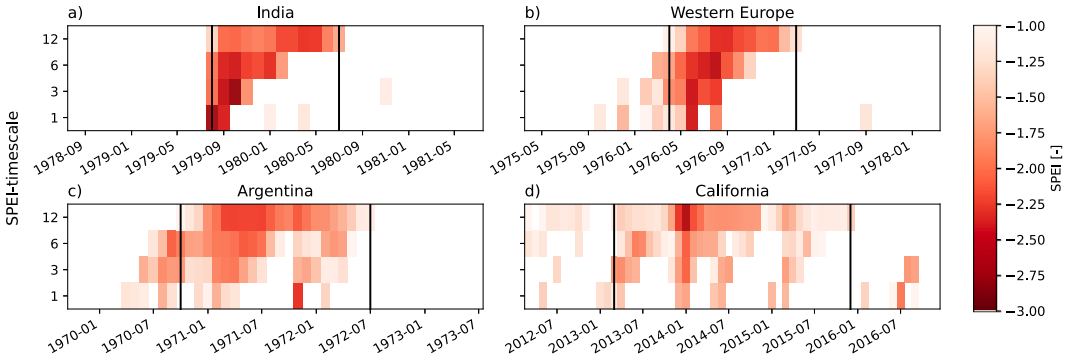

Fig. 4. Examples of MYDs with different development over time, indicated by SPEI-1, SPEI-3, SPEI-6, and SPEI-12 on the y-axis. On the x-axis, the dates from one year before the start of a MYD up to one year after the end of a MYD are shown. The start and end dates of the MYD itself are indicated with vertical black lines. Values above SPEI = −1 are masked for clarity. (a) Fast onset of MYD in India between 08-1979 and 07-1980; (b) Slow onset of MYD in Western Europe between 04-1976 and 03-1977; (c) Continuous MYD in Argentina between 10-1970 and 07-1972; (d) Reinforced MYD in California between 03-2013 and 12-2015.

as it takes time for a precipitation deficit or heightened evaporation to affect groundwater resources. The build-up to MYDs varies per region and is illustrated for four different MYDs in Fig. 4, where we define the propagation time as the period between the start of SPEI-1 ≤ -1 and the start of SPEI-12 ≤ -1. Generally, there are two different build-up scenarios for MYDs. Either they have a very sudden onset, or a longer build-up period of several months precedes them. Sudden onsets often follow a missed, reduced, or shortened wet season, and thus the affected regions miss out on a significant part of their annual precipitation. An example of this type of drought is shown in Fig. 4a for India, where SPEI-1, SPEI-3, SPEI-6 and SPEI-12 all have their onset in the same month. This propagation pattern is also observed in some MYDs in California and South Africa.

Longer propagation times are more common in regions with persistent precipitation levels throughout the year (see Fig. 1 for precipitation climatologies), where one dry month will not cause a MYD. This type of drought propagation pattern is more commonly found in Western Europe, Argentina, and Australia, with propagation times ranging between 3 and 9 months. An example from Western Europe is shown in Fig. 4b, where SPEI-1 drops below −1 for six months before SPEI-12 does. There is no distinction between regions with relatively fast or slow propagation times, as some regions experience a mix of them. In regions with a wet season, such as India, MYDs often form after two consecutive dry monsoon periods, where the first is insufficient to start the MYD but the second drought pushes the hydrological system into a MYD. California also has one MYD with a faster propagation time (Fig. 4d) and one with a slower propagation time, which is caused by the second MYD starting in an anomalously dry boreal summer. Similarly in South Africa, longer propagation times are associated with droughts that start in austral winter, which is their respective dry season.

Besides differences in initial development and their driving processes, we also observe differences in how MYDs are sustained over time. This MYD continuity can also be divided into two types. MYDs are either sustained by a continuous period of dry weather or constantly reinforced by new, shorter dry spells. In California, one of its two MYDs is caused by three consecutive dry boreal winters (Fig. 4d), which can be tracked from SPEI-1, prolonging the SPEI-12 to stay under −1. The other type is due to continuous dry circumstances starting in boreal summer. In Western Europe, MYDs typically start in winter and intensify in summer (as seen in Fig. 4b), except for the 2018–2019 MYD, which was caused by two consecutive dry summers. MYDs in India are less diverse and are all caused by either one or two missed or diminished monsoon seasons. Argentina experiences more variation, with MYDs caused by continuous droughts, consecutive dry winters, or a combination of a dry summer and a dry autumn. South Africa and Australia mostly experience continuous dry spells. An example of Argentina is shown in Fig. 4c, where the first year is continuously dry as measured by SPEI-1.

3.3. Direct drivers of MYDs

Having established the general characteristics of MYDs in the different focus regions, we turn to their direct drivers: precipitation and evaporation. The primary direct atmospheric drivers of MYDs are shown in Fig. 5 and vary per region, with precipitation and PET having different amplitudes. Starting with precipitation, India and Argentina exhibit the largest apparent differences between MYDs and NDs. In India, precipitation levels during MYDs are consistently lower than during NDs, indicating that precipitation is a key driver in differentiating between MYDs and NDs. In Argentina, MYDs and NDs begin with similar precipitation levels but diverge shortly after onset. During MYDs, precipitation continues to decline, whereas it recovers quickly during NDs. On average, precipitation levels are also lower during MYDs than during NDs for Western Europe and South Africa, but these differences are less pronounced due to overlapping individual MYD and ND events. No significant differences are observed in precipitation between MYDs and NDs for California and Australia.

When comparing PET between MYDs and NDs, Western Europe, Argentina, South Africa, and Australia start with similar values but diverge over time. The most significant difference is observed in Western Europe, where PET continues to increase during the first half-year of the MYDs, while it goes back to normal values during NDs, indicating that PET is an important direct atmospheric driver for MYDs in Western Europe. In South Africa, Australia, and to a lesser extent in Argentina, PET also increases during MYDs, while it stays at the initial value for NDs. In contrast, California and India show different relationships between the droughts and PET. In California, MYDs start with higher PET values than NDs, and PET grows at a similar rate during both types of droughts. The main difference is that PET continues to increase during MYDs, while NDs have already ended. India is the only region where PET is higher during NDs than during MYDs, making it clear that

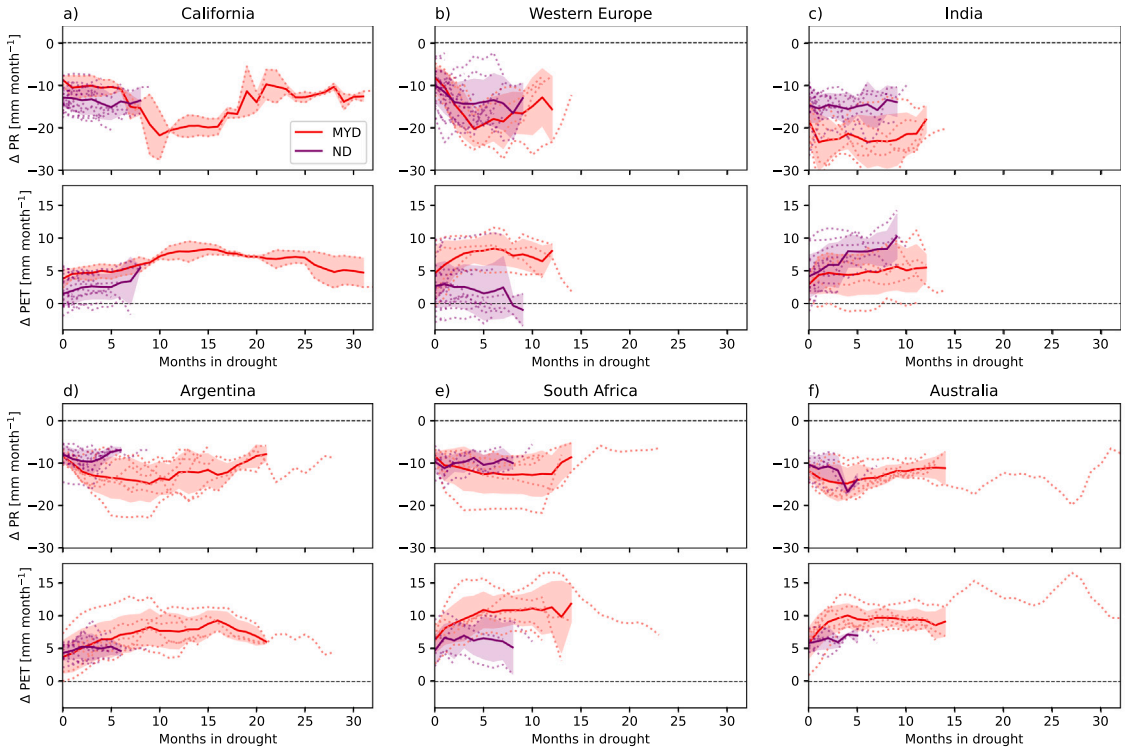

Fig. 5. Anomalies of precipitation (top) and potential evapotranspiration (bottom) during MYDs (red) and NDs (purple) in all six focus regions. A 12-month running mean was applied to all timeseries to remove seasonality and enable easier comparison with SPEI-12. Individual droughts are shown using dotted lines and their mean is plotted as a continuous line as long as multiple individual drought cases exist. Shading shows the standard deviations and a dashed black line shows the zero anomaly line. (For interpretation of the references to colour in this figure legend, the reader is referred to the web version of this article.)

PET is not the main driving factor in distinguishing between NDs and MYDs in India.

In short, all regions have anomalously low precipitation and high PET values during droughts, but it differs which factor is more pronounced in extending a ND to a MYD. Lower precipitation is likely the main driver for MYDs in India, while PET is more important in Western Europe and South Africa. For most regions except for PET in California, the lines for MYDs and NDs begin to diverge after starting from approximately equal anomalies. This implies that there are different atmospheric mechanisms which drive the development of MYDs or NDs. Besides the importance of the prevailing climate in which a region resides – Western Europe having a mid-latitude climate, India a monsoonal climate, while the others are experiencing influences of both – the reason behind these differences could be related to chance or longer-term external forcing, which we will revisit in Section 3.4.

The relation between SPEI-12 and precipitation, and SPEI-12 and PET is shown in Fig. 6. The linear regressions show the extent to which SPEI-12 is influenced by precipitation or PET, and how this relationship differs between the regions and types of drought. In Australia, both precipitation ($r^2 = 0.95$) and PET ($r^2 = 0.90$) have a strong linear correlation with SPEI-12 (Fig. 6a). This relation is less straightforward for both Western Europe (Fig. 6b) and California (Fig. 6c), which both have a strong linear correlation for precipitation ($r^2_{WEU} = 0.88$ and $r^2_{CAL} = 0.96$) while having a weaker correlation for PET ($r^2_{WEU} = 0.39$ and $r^2_{CAL} = 0.52$), indicating that a broader range of values is possible within NDs and MYDs. For all regions, PET has a bigger absolute impact on SPEI-12 than precipitation (e.g. $\alpha_{PET} = -0.16$ mm month^{-1} versus $\alpha_{PR} = -0.10$ mm month^{-1} for AUS and WEU), but it has to be noted that the range of variation is bigger in precipitation than PET, making it hard to compare the different components. Generally, the slope of the regression line is larger and the correlation is higher (except for precipitation in AUS) during MYDs than during NDs for both PET and precipitation, indicating that the influence of PET and precipitation is stronger during MYDs than during NDs, but this interpretation is affected by the hard cut-off at SPEI-12 = −1, high variability in data, and limited drought events. Note that at both extreme ends of SPEI-12, towards 3 and -3, a deflection from the linear regression is visible due to the standardization process involved in calculating SPEI-12. Because of this capping, the slope of the linear regression for both types of droughts is less steep compared to the whole spectrum of SPEI-12. This effect can be seen in all six focus regions.

For some regions, the values for precipitation and PET during MYDs exceed those of NDs and non-drought conditions, leading to threshold values above or below which the probability of a MYD is high. These threshold values are useful indicators for differentiation between MYDs and NDs and thus for MYD predictability. Especially for PET in Australia, the difference between the position of MYDs and NDs on the x-axis is visible (Fig. 6a), as MYDs occur at far higher values of PET than NDs. This indicates that if a year trespasses a certain PET threshold in this historical record, it is likely part of a MYD. Similar results are found for India, but for precipitation instead of PET (see SI Section S.6). This difference is not as prominent for precipitation in Australia, where precipitation levels of MYDs largely overlap with those of NDs. As a result, no absolute distinction can be made between precipitation values of MYDs and NDs, but only a heightened chance towards lower extreme precipitation values. The result that PET is more important in distinguishing between NDs and MYDs for Australia, aligns with results from Fig. 5. For Western Europe, we can draw a similar conclusion as for precipitation in Australia; both precipitation and PET are important in forming MYDs, however, there is no clear distinction between PET and precipitation values in NDs and MYDs. Even though Fig. 5b showed the difference in PET during MYDs and NDs and the probability of MYDs is high for higher PET values in Fig. 6b, it does not lead to a clear cut-off value. For California (similar for ARG and SA, see SI Section S.6), both precipitation and PET have threshold values for MYDs, although they are limited to their respective lowest and highest values.

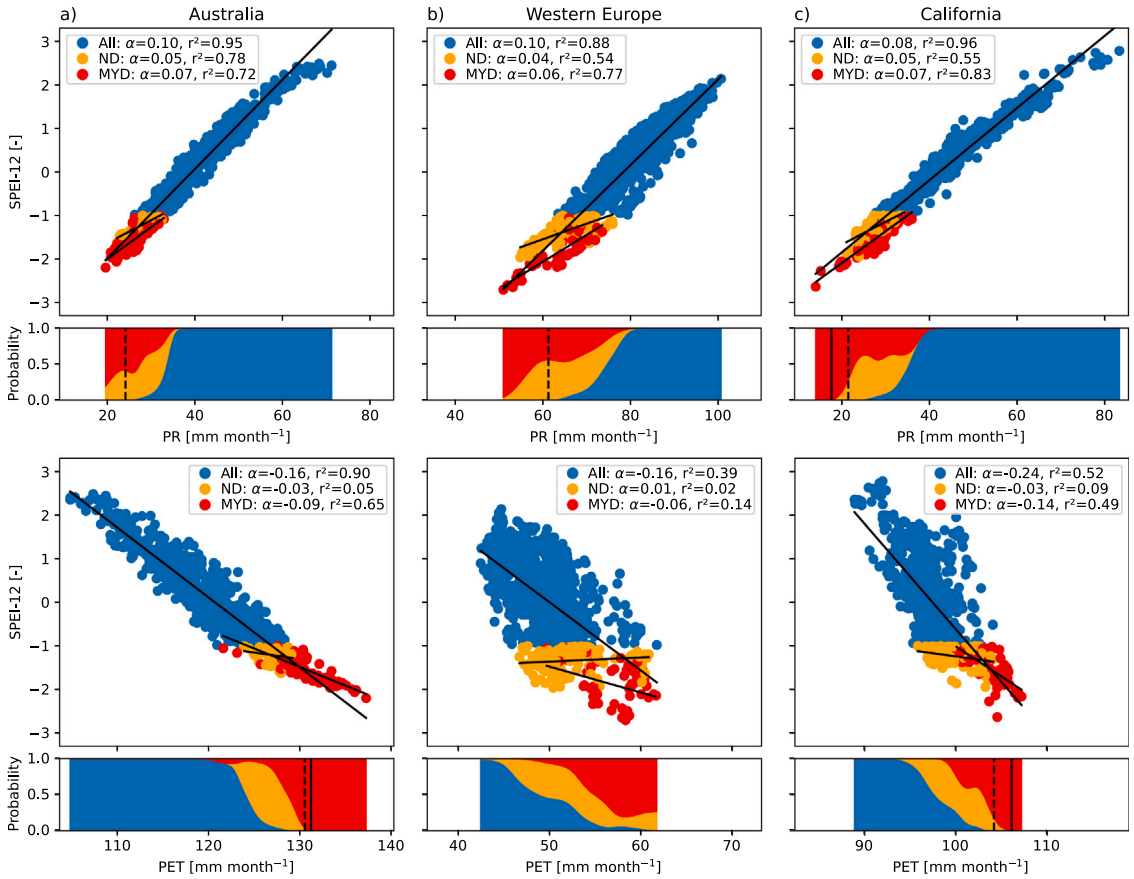

Fig. 6. Linear regression of SPEI-12 against the 12-month rolling mean of precipitation (PR, top) and potential evapotranspiration (PET, below) for Australia (a), Western Europe (b), and California (c). The legends state the slope (α, in mm month^{-1}) and variance (r^2) of the linear regressions. Blue dots indicate all months not in drought, orange for all months in NDs, and red for all months in MYDs. Note dots overlap and hide others, to avoid complete coverage we have plotted the months of MYDs and NDs in random order. Underneath each linear regression plot, the probability for each type of drought is shown per value of precipitation and PET. The dashed vertical line indicates the value where the probability of no drought is 0, and the continuous vertical line shows where the probability of MYDs is 1. (For interpretation of the references to colour in this figure legend, the reader is referred to the web version of this article.)

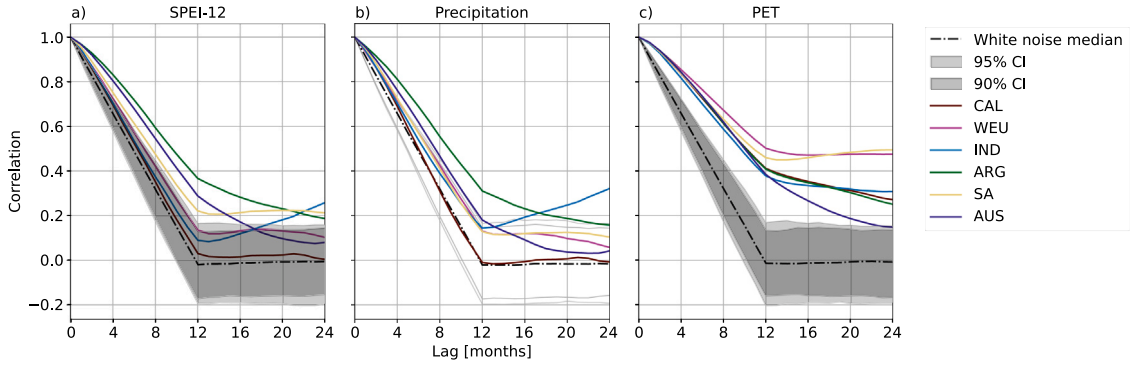

Fig. 7. Lagged auto-correlations of the SPEI-12 (a), precipitation (b), and PET (c) time series for each region (colours indicated in the legend), joined by the white noise median, its 95% and 90% confidence intervals (CI). The white noise band has no long-term memory by definition. (For interpretation of the references to colour in this figure legend, the reader is referred to the web version of this article.)

3.4. Long-term memory in SPEI-12

In Fig. 7, the persistence of SPEI-12, precipitation, and PET is compared to that of white noise for each of the six focus regions. Regions falling within the white noise band have little to no predictive potential in the months preceding a specific moment in time, as white noise has no long-term memory by definition. For SPEI-12 (Fig. 7a), we observe a distinction between the focus regions on the NH and SH. Ordered from higher to lower correlation, Argentina, Australia, and South Africa are found outside the 95% confidence interval of white noise, while Western Europe, India, and California fall within the 90% confidence interval. More specifically, Western Europe is near the upper edge of the 90% interval, and India and California are closer to the white noise medium. Persistence and therefore potential predictability in SPEI-12 is thus higher in the SH focus regions than in the NH regions. When SPEI-12 is broken down into precipitation

and PET, notable differences emerge. For precipitation (Fig. 7b), only Argentina is completely outside the confidence interval, with Australia just on the upper boundary of the 95% interval. Western Europe, India and South Africa are all on the upper side of the 90% interval, while California resembles the white noise median. For PET (Fig. 7c), all regions are outside the confidence intervals, with Western Europe and South Africa having the highest values, followed by Argentina and California, and then India and Australia. This indicates that PET has a higher predictive value than precipitation for all regions. For the regions that exhibit predictability in SPEI-12, we observe that the predictability for Argentina is likely a combination of precipitation and PET predictability, while for Australia and South Africa this most likely comes from the PET anomalies. In all other regions, there is insufficient potential predictability in the combination of precipitation and PET to result in potential predictability in SPEI-12.

4. Discussion

In this study, we base our MYD event selection on consecutive periods in SPEI-12 timeseries below a certain threshold. In SPEI-12, the calculation of PET and its ability to reflect the actual water loss to the atmosphere is the largest source of uncertainty. We have computed PET using the Penman-Monteith (FAO56) equation, which assumes a stable atmospheric boundary layer and an Earth's surface covered by 0.12 m crop height or grassland. This approach, while widely accepted, neglects the presence of other vegetation types and convection in the lower atmosphere (Zotarelli et al., 2010). Moreover, PET tends to be less representative of the actual evapotranspiration in arid regions, due to the discrepancy between available water for evapotranspiration and atmospheric demand (Hua et al., 2020). Milly and Dunne (2017) compared different PET methods, and concluded that they all overestimate the actual evapotranspiration, although in different quantities. However, comparing the PET method with the lowest bias ("energy-only") to Penman-Monteith used here only results in minor differences in SPEI-12, as can be seen in SI Section S.5. Next to the physical inaccuracies, the use of PET on daily timescales leads to biases caused by the non-linear character of turbulent transport of heat fluxes, which vary throughout the day. This variation means that taking longer time steps will lead to biases (Han et al., 2024). Ideally, the calculation of evapotranspiration thus requires local and hourly calibration or direct measurements, which is an active but unfinished area of study (Anabalón and Sharma, 2017). The major advantage of using Penman-Monteith is that it is based on the physical principles of energy balance and mass transportation, which can be calculated directly from a large collection of meteorological variables otherwise excluded. Additionally, SPEI-12 allows us to compare different climatic regions over time because of its standardization. The choice of threshold in the MYD definition is also an important aspect of the MYD characterization. The regions with a higher resemblance in duration between NDs and MYDs are more susceptible to threshold-based decisions in the MYD definition. For instance, an 11 month-during ND following from our SPEI-12 = −1 threshold may have been counted as a MYD given a more relaxed threshold. Conversely, regions with clear distinctions between NDs and MYDs are less affected by minor threshold adjustments, as slight changes in thresholds will not change the categorization. This effect is also observed in SI Section S.4 where we compare the different reanalysis products; the agreement is lower for shorter or less intense MYDs than it is for more intense MYDs. For regions as California the severity of the last (only) two MYDs influences the standardization process significantly. Even though there have been more long-lasting intense droughts before 2010 (Christian-Smith et al., 2011; Richman and Leslie, 2015), they do not compare to the MYDs of 2013–2015 and 2020–2022 in intensity, and are therefore reduced to 'normal droughts'.

Another important factor affecting interpretation in this study is the limited number of MYD events, constrained by both the study's timeframe (1950–2023) and the inherent anomalous behaviour of MYDs. This timeframe is the period most covered by reanalysis products, whereas observations prior to 1950 were more scarce. The low number of MYDs is a limiting factor in creating understanding and identifying the drivers of MYDs in this study. Especially for California, where only two MYD events were found within this record, the representation of what kinds of MYDs are possible is limited, influencing the interpretation of the results. In contrast, Argentina and Australia each experienced six MYD events, providing a broader perspective on MYD probabilities, behaviour, and drivers. Except for a few MYDs in the 1950s, all MYDs in our dataset are represented in literature (Table A.1), giving confidence in the coverage and accuracy of the MYD dataset. In future work we plan to expand this using climate models participating in CMIP6. Moving from the methodology to the interpretation of our results, we find that the mid-latitude climate (WEU) and monsoonal climate (IND) seem to differentiate less between NDs and MYDs in both duration and drivers compared to climates which are subject to a mix of (sub)tropical and mid-latitudinal influences (AUS, ARG, SA, CAL). The combined information on drought duration and PET/precipitation threshold leads us to expect more pronounced differences or consistency in drivers playing a key role in the development of MYDs compared to NDs. Especially if the consistency of the drivers turns out to be the key difference, slower varying climate indices such as (remote) sea surface temperatures, soil moisture content, and snow cover could play an important role in providing more favourable MYD conditions, potentially leading to higher predictability for MYDs when such drivers can be identified (Krishnamurthy, 2019).

Indicators of predictability were found in Argentina, Australia, and South Africa, where autocorrelated SPEI-12 signals were detected. For these regions, it is known that teleconnections such as the El Niño Southern Oscillation (ENSO) and Indian Ocean Dipole (IOD) significantly influence regional water cycles and can increase the chance of droughts occurring (Reddy et al., 2022; Araneda-Cabrera et al., 2021; Chikoore and Jury, 2021). For example, the 2015–2017 MYD in South Africa has been linked to a major El Niño event happening simultaneously (Kolusu et al., 2019), and the MYDs in the early 2000s in Australia were driven by negative IODs (Ummenhofer et al., 2009). Therefore, these climate indices could also act as potential predictors of MYDs. Dissecting SPEI-12 into its separate components revealed that potential predictability coming from precipitation anomalies is limited, except for Argentina. The low potential predictability in precipitation for India could be influenced by the variations in its monsoonal climate. However, indicators for the strength of these monsoons have been found by several studies. Kumar et al. (2013) showed that monsoon droughts are often influenced by ENSO, and worsened by increased sea surface temperatures in the Indian Ocean forced by global warming. Borah et al. (2020) filled the knowledge gaps on monsoon droughts that happened during years when no ENSO forcing was present, by finding an atmospheric teleconnection between cold ocean anomalies in the North Atlantic and Rossby wave trains curving towards India. A lack of persistence in precipitation therefore does not always equal an absence of predictability.

In contrast to precipitation, PET shows greater predictive potential, although these relations may be influenced by trends in different components of PET under the influence of anthropogenic climate change, as significant upward trends are present in e.g. $t2m$ (see SI Section S.7). The potential predictability of PET is highest in Western Europe, possibly due to land-atmosphere interactions leading to positive feedbacks (Dirmeyer et al., 2021). It is also the only energy-limited region, whereas the other regions are more water-limited, and therefore an increase in PET during MYDs could have a higher influence here (Ruijsch et al., 2024). However, Van der Wiel et al. (2023) did not find any indicators of predictability for MYDs in Western Europe, which is reflected in Fig. 7a, where SPEI-12 for Western Europe falls within the white noise band. Even though this analysis shows potential for predictability for the overall SPEI-12, precipitation and PET time series for some regions, it does not distinguish between the predictability of

MYDs, NDs, or other periods in time.

Multiple regions exhibit multi-decadal variations between wetter and drier periods, which influence the likelihood of MYDs. These variations can be driven by multi-decadal climate variations, such as the Pacific Decadal Oscillation (PDO) or the Atlantic Multidecadal Oscillation (AMO). These decadal variations switch between modes of warm and cold ocean basin anomalies and affect atmospheric weather patterns and thereby modulate drought probabilities (Jones and Carvalho, 2018; Ionita et al., 2012; Vijverberg and Coumou, 2022). Especially for Argentina, the dry and wet phases coincide with the cold (before 1977 and after 2003) and warm (between 1977 and 2003) phases of the PDO respectively. This correlation between a cold PDO phase and drought in Argentina has also been demonstrated by Nguyen et al. (2021), and similarly for Australia and South Africa caused by the extended version of the PDO, the Interdecadal Pacific Oscillation (IPO), and the Southern Annual Mode (SAM) (Kiem and Franks, 2004; Malherbe et al., 2016) .

Notably, the last two decades of the SPEI-12 time series indicate widespread dryness across all regions. While this could result from multi-decadal oscillations, it can also be the result of anthropogenic climate change leading to favourable conditions for droughts and multi-year droughts by impacting precipitation and evaporation levels or variability. Especially in California, where no MYDs were found in this dataset before 2010, it has been shown by both Cook et al. (2018) and Diffenbaugh et al. (2015) that climate change played a key role in the two recent MYDs. Also in Australia, Falster et al. (2024) showed that it is likely that future multi-year droughts will be more intense and will last longer due to anthropogenic climate change. In contrast, no clear trend is visible in India, where a wet period before 1965 may reflect a bias in ERA5 precipitation data, resulting in higher precipitation values compared to different observational records (SI Figure S3). This bias in precipitation in the lower latitudes is a known shortcoming of the ERA-5 precipitation data, which is partly due to a lack of observations in this area combined with models having more difficulty reproducing accurate tropical rainfall patterns (Lavers et al., 2022) (see SI Section S.3). Furthermore, the low agreement between SPEI-12 timeseries derived from different reanalysis datasets (Figure S7) reduces the reliability of results for India. While biases and discrepancies do exist in other regions, these differences are less pronounced. Most importantly, the different reanalysis datasets agree on the largest MYDs for these areas and mainly differ for less intense MYDs residing closer to SPEI = −1.

5. Conclusion

This study provides an analysis of the characteristics and drivers of multi-year droughts in different climate regions represented by California, Western Europe, India, central Argentina, South Africa, and Southeast Australia. Using ERA5 reanalysis data, we calculated the SPEI-12 drought index to characterize droughts. Multi-year droughts were defined as those periods in time where SPEI-12 was below −1 for 12 consecutive months, while droughts with SPEI-12 below −1 for shorter amounts of time are classified as normal droughts. Our findings reveal regional differences in the occurrence, duration, onset, and predictability of multi-year droughts between the focus regions. Multi-year droughts play a larger role in the focus regions in the southern hemisphere, where the majority of the time spent in drought is taken up by multi-year droughts, in contrast to the regions in the northern hemisphere. In California, central Argentina and Australia, multi-year droughts and shorter ‘normal’ droughts show a clear distinction in duration. In contrast, multi-year droughts form the extreme right tail outliers in the drought duration distribution for the other regions. This suggests that larger differences in drivers of normal droughts and multi-year droughts exist for regions subject to a mix of (sub)tropical and mid-latitudinal influences compared to mid-latitudinal and monsoonal climates. We observed that the onset times of multi-year droughts vary between regions with seasonal rainfall patterns and those with steady precipitation throughout the year. Regions with seasonal rainfall patterns tend to experience sudden onsets of multi-year droughts which are caused by a diminished or shortened wet season, while extended or worsened dry seasons result in longer onset times. Regions with more uniform precipitation patterns generally have longer onset times, as they require more consecutive dry months to trigger a multi-year drought event.

In terms of direct drivers, our study found that most regions depend on both limited precipitation and elevated evapotranspiration. For some regions, however, one of these drivers is the dominating factor. For California, positive anomalies in potential evapotranspiration are the key driver, while for India, negative anomalies in precipitation are more important. Initially, multi-year droughts and normal droughts share similar drivers, but these drivers often diverge over time. By examining the absolute precipitation and potential evaporation values, we identified regional thresholds that either distinctly separate the drivers of normal drought and those of multi-year droughts, or indicate heightened probabilities of multi-year droughts. Clear distinctions between multi-year droughts and normal droughts were identified for California, central Argentina, and South Africa, where the exceedance of precipitation and potential evapotranspiration thresholds resulted in multi-year droughts. In India, a threshold was found solely for precipitation, while in Australia only potential evapotranspiration was identified as a determining factor. For Western Europe, we found an increased probability of multi-year droughts for both high PET values and low precipitation, but no clearly defined thresholds. Furthermore, the potential for long-term predictability of multi-year droughts was observed through the autocorrelation of SPEI-12 in central Argentina, South Africa, and Australia. Further research is needed to translate this persistence in SPEI-12 to the actual predictability of multi-year droughts compared to normal droughts.

The insights gained from this study are crucial for science and for informing drought management policies, as drought mitigation approaches will differ depending on the expected duration of the drought event. The current methodology can be easily adjusted and expanded to other regions in the world. Further research could improve the current results by analysing longer time series by using extended observational records based on proxies, or simulated time series from climate modelling experiments. This would lead to a larger sample size of multi-year droughts in the analysis, improving the statistical significance of the results. Additionally, expanding knowledge of long-term predictability in local drivers coming from the oceans, dynamics in the atmosphere, or other teleconnections that can increase the chances and predictability of multi-year droughts is important. Improving this knowledge is vital to better navigate the societal and ecological impacts of multi-year droughts.

CRediT authorship contribution statement

Jonna van Mourik: Writing – original draft, Visualization, Validation, Software, Methodology, Formal analysis, Data curation, Conceptualization. **Denise Ruijsch:** Validation, Software, Methodology, Data curation. **Karin van der Wiel:** Writing – review & editing, Formal analysis, Conceptualization. **Wilco Hazeleger:** Writing – review & editing, Formal analysis, Conceptualization. **Niko Wanders:** Writing – review & editing, Project administration, Funding acquisition, Formal analysis, Conceptualization.

Code and data availability

Data: https://doi.org/10.24416/UU01-MQT1NN
Code: https://zenodo.org/doi/10.5281/zenodo.13709945

Declaration of competing interest

The authors declare that they have no conflict of interest.

Acknowledgements

Funded/Co-funded by the European Union (ERC, MultiDry, Grant Agreement number: 101075354). Views and opinions expressed are however those of the author(s) only and do not necessarily reflect those of the European Union or the European Research Council. Neither the European Union nor the granting authority can be held responsible for them. JvM, DR and NW are supported by the ERC STG MultiDry project.

Appendix A. MYDs overview

See Table A.1.

Appendix B. Extended method: SPEI and PET formulas

In Section 2 the basic principles of the Standardised Precipitation-Evapotranspiration Index (SPEI) (Vicente-Serrano et al., 2010; Bourgault et al., 2023) and the Penman-Monteith (FAO56) potential evapotranspiration (PET) (Zotarelli et al., 2010; Penman, 1948; Monteith, 1965) are explained. In this appendix we will provide more details on the formulas and assumptions used for these indices.

B.1. SPEI

SPEI was originally constructed by Vicente-Serrano et al. (2010). The *xclim* package of Bourgault et al. (2023) follows their paper, though by using numerical methods instead of the approximations for the parameters α, β and γ used in the original paper. SPEI is based on the water balance, which is calculated by subtracting the potential evapotranspiration from the precipitation per month j in year i:

$$D_{i,j} = P_{i,j} - PET_{i,j}. \tag{B.1}$$

The calculated $D_{i,j}$ values are aggregated for the timescale of choice, leading to $D^k_{i,j}$ for a given month j, year i and chosen timescale k, which is 12 in this paper. The package takes the sum of a sliding window over this timescale k, such that every $D^k_{i,j}$ represents the accumulated state of the water balance over the past k months for a certain time.

In Vicente-Serrano et al. (2010) multiple probability distributions were tested and the log–logistic probability distribution resulted in the best fit for low values of D. This three-parameter distribution with $D^k_{i,j}$ filled in looks like

$$F(D^k_{i,j}) = [1 + (\frac{\alpha}{D^k_{i,j} - \gamma})^{\beta}]^{-1}, \tag{B.2}$$

where α, β and γ are the scale, shape and origin parameters respectively. In Vicente-Serrano et al. (2010) these parameters are obtained following Singh et al. (1993), but the package of Bourgault et al. (2023) estimates these parameters for every gridcell separately for elevated precision. To arrive at the final SPEI value, the probability distribution function is standardized using the inverse cumulative distribution of the reference distribution (Φ^{-1}):

$$\text{SPEI-k}_{i,j} = \Phi^{-1}(F(D^k_{i,j})). \tag{B.3}$$

This standardization is done with respect to a certain calibration period, which is the period of 1950–2020 for this paper. Over this period, the mean value of SPEI is zero and the standard deviation is one; positive values denote wet periods, and negative values denote dry periods.

B.2. PET

Following Zotarelli et al. (2010), PET is calculated by the *pyet* package (Vremec et al., 2023) as

$$PET = \frac{0.408\Delta(R_n - G) + \gamma \frac{900}{T+273} u_2 (e_s - e_a)}{\Delta + \gamma(1 + 0.34u_2)}. \tag{B.4}$$

The variables from this equation are explained in Table 2, where it is also stated which ERA5 variables are included. Here we will elaborate on the exact formulas used to go from the ERA5 variables to the variables needed for Eq. (B.4).

The net radiation R_n is calculated from the net solar radiation R_s (*ssr* in ERA5) and net thermal radiation R_t (*str* in ERA5)

$$R_n = R_s + R_t. \tag{B.5}$$

The total wind velocity needs to be calculated from its zonal ($u10$ in ERA5) and meridional ($v10$ in ERA5) wind velocity:

$$u_{tot,10} = \sqrt{u^2_{10} + v^2_{10}}. \tag{B.6}$$

However, since ERA5 only provides wind velocities at 10 m height, this velocity still needs to be adjusted to 2 m height. This is done following Allen (1998), with $z = 10$ m

$$u_2 = u_{tot,z} \frac{4.87}{log(67.8z - 5.42)}. \tag{B.7}$$

The vapour pressure is calculated both for air temperature T ($t2m$ in ERA5), which is referred to as the saturated vapour pressure e_s, and for the dewpoint temperature T_{dew} ($d2m$ in ERA5), which is referred to as the actual vapour pressure e_a:

$$e_s(T) = 0.6108 \exp(\frac{17.27T}{T + 237.3}) \tag{B.8}$$

$$e_a(T_{dew}) = 0.6108 \exp(\frac{17.27T_{dew}}{T_{dew} + 237.3}) \tag{B.9}$$

They can be calculated by either taking the mean temperature, or by taking the average vapour pressure following from using the minimum and maximum temperature. All temperatures are in [°C] here.

Lastly, the slope of the vapour pressure curve Δ and the psychometric constant γ are needed. Δ is calculated using the air temperature T:

$$\Delta = \frac{4098[0.6108 \exp(\frac{17.27T}{T+237.3})]}{(T + 237.3)^2}, \tag{B.10}$$

and γ is calculated using the surface pressure P (sp in ERA5):

$$\gamma = \frac{c_p P}{\epsilon \lambda} = 0.665 \cdot 10^{-3} P. \tag{B.11}$$

The other variables and constants are λ for latent heat of vaporization, which has an average value of 2.45 [MJ kg^{-1}], but is based on the actual temperature by the package; c_p for specific heat at constant temperature, with a value of $1013 \cdot 10^{-3}$ [MJ kg^{-1} °C^{-1}], and ϵ for the ratio of molecular weight of water vapour divided by dry air, with a value of 0.622.

Appendix C. Supplementary data

Supplementary material related to this article can be found online at https://doi.org/10.1016/j.wace.2025.100748.

Data availability

DOI code for the data is stated in the paper
Data: https://doi.org/10.24416/UU01-MQT1NN.

Table A.1
MYD events in the ERA5 period, based on the SPEI-12 timeseries and criterion (Fig. 2). Shown are starting date (MM-YYYY), end date, and total duration (months). Some proof of occurrence is provided by means of a literature overview that discusses these events, this overview is not meant to be complete, further literature on specific events might exist. If the same literature accounts for multiple MYDs in a row, this is indicated by "" for the next MYD.

Focus region	Start date	End date	Duration [months]	Literature
CAL	03-2013	12-2015	34	Luo et al. (2017), He et al. (2017) and Bales et al. (2018)
	05-2020	12-2022	32	Liu et al. (2022)
WEU	06-1959	08-1960	15	Van der Wiel et al. (2023)
	04-1976	03-1977	12	Perry (1976)
	08-2003	07-2004	12	Benedict et al. (2021)
	09-2018	09-2019	13	Rakovec et al. (2022) and Van der Wiel et al. (2021, 2023)
IND	08-1979	07-1980	12	Monirul Qader Mirza (2005)
	07-1982	06-1983	12	Mishra et al. (2019)
	06-1987	06-1988	12	Sinha et al. (2011) and Mishra et al. (2019)
	03-1992	05-1993	15	Monirul Qader Mirza (2005)
	06-2009	06-2010	13	Dharpure et al. (2022)
ARG	08-1955	10-1956	15	Barrucand et al. (2007)
	10-1970	07-1972	22	Morales et al. (2020) and Moraes et al. (2021)
	01-2009	02-2010	14	Garreaud et al. (2017) and Sgroi et al. (2021)
	05-2011	08-2012	16	""
	09-2019	01-2022	29	Naumann et al. (2023), Arias et al. (2024) and Moraes et al. (2021)
	03-2022	≥12-2023	≥22	""
SA	01-1954	02-1955	14	
	02-1956	01-1957	12	
	02-2013	02-2014	12	Malherbe et al. (2016)
	11-2015	01-2017	15	Malherbe et al. (2020), Chikoore and Jury (2021) and Pascale et al. (2021)
	10-2018	09-2020	24	Chikoore and Jury (2021)
AUS	09-1951	10-1952	14	
	08-1957	10-1958	15	Lindesay (2005)
	10-2002	09-2003	12	Leblanc et al. (2009) and Van Dijk et al. (2013)
	09-2006	10-2007	14	""
	03-2013	03-2014	13	Spinoni et al. (2019)
	09-2017	07-2020	35	Kumar et al. (2021) and King et al. (2020)

References

Adler, Robert F, et al., 2018. The Global Precipitation Climatology Project (GPCP) monthly analysis (new version 2.3) and a review of 2017 global precipitation. Atmosphere 9 (4), 138.

Allen, Richard G., 1998. Crop evapotranspiration. FAO Irrig. Drain. Pap. 56, 60–64.

Anabalón, Alfonso, Sharma, Ashish, 2017. On the divergence of potential and actual evapotranspiration trends: An assessment across alternate global datasets. Earth's Futur. 5 (9), 905–917.

Araneda-Cabrera, Ronnie J, Bermúdez, María, Puertas, Jerónimo, 2021. Benchmarking of drought and climate indices for agricultural drought monitoring in Argentina. Sci. Total Environ. 790, 148090.

Arias, Paola A, et al., 2024. Interplay between climate change and climate variability: the 2022 drought in Central South America. Clim. Change 177 (1), 6.

Bachmair, Sophie, et al., 2016. Drought indicators revisited: the need for a wider consideration of environment and society. Wiley Interdiscip. Rev.: Water 3 (4), 516–536.

Bales, Roger C, et al., 2018. Mechanisms controlling the impact of multi-year drought on mountain hydrology. Sci. Rep. 8 (1), 690.

Barrucand, M.G., Vargas, W.M., Rusticucci, M.M., 2007. Dry conditions over Argentina and the related monthly circulation patterns. Meteorol. Atmos. Phys. 98, 99–114.

Benedict, Imme, et al., 2021. Anomalous moisture sources of the Rhine basin during the extremely dry summers of 2003 and 2018. Weather. Clim. Extrem. 31, 100302.

Borah, Pritam Jyoti, et al., 2020. Indian monsoon derailed by a North Atlantic wavetrain. Sci. 370 (6522), 1335–1338.

Bourgault, Pascal, et al., 2023. Xclim: xarray-based climate data analytics. J. Open Source Softw. 8 (85), 5415.

Brunner, Manuela I., Tallaksen, Lena M., 2019. Proneness of European catchments to multiyear streamflow droughts. Water Resour. Res. 55 (11), 8881–8894.

Burls, Natalie J, et al., 2019. The Cape Town "day zero" drought and Hadley cell expansion. Npj Clim. Atmos. Sci. 2 (1), 27.

Chikoore, Hector, Jury, Mark R., 2021. South African drought, deconstructed. Weather. Clim. Extrem. 33, 100334.

Christian-Smith, Juliet, et al., 2011. Impacts of the California Drought from 2007 to 2009. Pacific Institute Oakland, CA, USA.

Cook, Benjamin, Mankin, Justin, Anchukaitis, Kevin, 2018. Climate change and drought: From past to future. Curr. Clim. Chang. Rep. 4, 164–179.

Cornes, R., et al., 2018. An ensemble version of the E-OBS temperature and precipitation datasets. J. Geophys. Res. Atmos. 123, http://dx.doi.org/10.1029/2017JD028200.

Dettinger, Michael D, et al., 2011. Atmospheric rivers, floods and the water resources of California. Water 3 (2), 445–478.

Dharpure, Jaydeo K, et al., 2022. Drought characterization using the combined terrestrial evapotranspiration index over the Indus, Ganga and Brahmaputra river basins. Geocarto Int. 37 (4), 1059–1083.

Diffenbaugh, Noah S., Swain, Daniel L., Touma, Danielle, 2015. Anthropogenic warming has increased drought risk in California. Proc. Natl. Acad. Sci. 112 (13), 3931–3936.

Dirmeyer, Paul A, et al., 2021. Land-atmosphere interactions exacerbated the drought and heatwave over northern Europe during summer 2018. AGU Adv. 2 (2), e2020AV000283.

Falster, Georgina M, et al., 2024. Potential for historically unprecedented Australian droughts from natural variability and climate change. Hydrol. Earth Syst. Sci. 28 (6), 1383–1401.

Funk, Chris, et al., 2015. The climate hazards infrared precipitation with stations—a new environmental record for monitoring extremes. Sci. Data 2 (1), 1–21.

García-Valdecasas Ojeda, Matilde, et al., 2021. Assessing future drought conditions over the Iberian Peninsula: the impact of using different periods to compute the SPEI. Atmosphere 12 (8), 980.

Garreaud, René D, et al., 2017. The 2010–2015 megadrought in central Chile: Impacts on regional hydroclimate and vegetation. Hydrol. Earth Syst. Sci. 21 (12), 6307–6327.

Gelaro, Ronald, et al., 2017. The modern-era retrospective analysis for research and applications, version 2 (MERRA-2). J. Clim. 30 (14), 5419–5454.

Gessner, Claudia, et al., 2022. Multi-year drought storylines for Europe and North America from an iteratively perturbed global climate model. Weather. Clim. Extrem. 38, 100512.

Gupta, Vivek, Jain, Manoj Kumar, 2018. Investigation of multi-model spatiotemporal mesoscale drought projections over India under climate change scenario. J. Hydrol. 567, 489–509.

Han, Jeongwoo, Singh, Vijay P., 2023. A review of widely used drought indices and the challenges of drought assessment under climate change. Environ. Monit. Assess. 195 (12), 1438.

Han, Yizhi, et al., 2024. Evaluating biases in Penman and Penman–Monteith evapotranspiration rates at different timescales. J. Hydrol. 131534.

He, Minxue, Russo, Mitchel, Anderson, Michael, 2017. Hydroclimatic characteristics of the 2012–2015 California drought from an operational perspective. Climate 5 (1), 5.

Hersbach, H., et al., 2023. ERA5 hourly data on single levels from 1940 to present. In: Copernicus Climate Change Service (C3S) Climate Data Store (CDS). http://dx.doi.org/10.24381/cds.adbb2d47 (Accessed 04 2024).

Hua, Ding, et al., 2020. Uncertainty assessment of potential evapotranspiration in arid areas, as estimated by the Penman-Monteith method. J. Arid. Land 12, 166–180.

Huffman, G.J., et al., 2023. GPM IMERG Final Precipitation L3 1 month 0.1 degree x 0.1 degree V07. Goddard Earth Sciences Data and Information Services Center (GES DISC), http://dx.doi.org/10.5067/GPM/IMERG/3B-MONTH/07, (Accessed [to do]).

Ionita, Monica, et al., 2012. Interannual to decadal summer drought variability over Europe and its relationship to global sea surface temperature. Clim. Dyn. 38, 363–377.

Japan Meteorological Agency, 2023. Japanese Reanalysis for Three Quarters of a Century (JRA-3Q). Boulder CO, URL: https://doi.org/10.5065/AVTZ-1H78.

Jones, Charles, Carvalho, Leila M.V., 2018. The influence of the Atlantic multidecadal oscillation on the eastern Andes low-level jet and precipitation in South America. NPJ Clim. Atmos. Sci. 1 (1), 40.

Kiem, Anthony S., Franks, Stewart W., 2004. Multi-decadal variability of drought risk, eastern Australia. Hydrol. Process. 18 (11), 2039–2050.

King, Andrew D, et al., 2020. The role of climate variability in Australian drought. Nat. Clim. Chang. 10 (3), 177–179.

Kolusu, Seshagiri Rao, et al., 2019. The El Niño event of 2015–2016: climate anomalies and their impact on groundwater resources in East and Southern Africa. Hydrol. Earth Syst. Sci. 23 (3), 1751–1762.

Kreibich, Heidi, et al., 2022. The challenge of unprecedented floods and droughts in risk management. Nat. 608 (7921), 80–86.

Krishnamurthy, Venkataramanaiah, 2019. Predictability of weather and climate. Earth Space Sci. 6 (7), 1043–1056.

Kumar, K Niranjan, et al., 2013. On the observed variability of monsoon droughts over India. Weather. Clim. Extrem. 1, 42–50.

Kumar, Sujay V, et al., 2021. The 2019–2020 Australian drought and bushfires altered the partitioning of hydrological fluxes. Geophys. Res. Lett. 48 (1), e2020GL091411.

Lavers, David A, et al., 2022. An evaluation of ERA5 precipitation for climate monitoring. Q. J. R. Meteorol. Soc. 148 (748), 3152–3165.

Leblanc, Marc J, et al., 2009. Basin-scale, integrated observations of the early 21st century multiyear drought in southeast Australia. Water Resour. Res. 45 (4).

Lesk, Corey, et al., 2022. Compound heat and moisture extreme impacts on global crop yields under climate change. Nat. Rev. Earth Environ. 3 (12), 872–889.

Lindesay, Janette A., 2005. Climate and drought in the subtropics: the Australian example. In: From Disaster Response To Risk Management: Australia's National Drought Policy. Springer, pp. 15–36.

Liu, Pang-Wei, et al., 2022. Groundwater depletion in California's Central Valley accelerates during megadrought. Nat. Commun. 13 (1), 7825.

Luo, Lifeng, et al., 2017. Contribution of temperature and precipitation anomalies to the California drought during 2012–2015. Geophys. Res. Lett. 44 (7), 3184–3192.

Malherbe, Johann, et al., 2016. South African droughts and decadal variability. Nat. Hazards 80, 657–681.

Malherbe, Johan, et al., 2020. Recent droughts in the Kruger National Park as reflected in the extreme climate index. Afr. J. Range Forage Sci. 37 (1), 1–17.

Milly, P.C.D., Dunne, Krista A., 2017. A hydrologic drying bias in water-resource impact analyses of anthropogenic climate change. JAWRA J. Am. Water Resour. Assoc. 53 (4), 822–838.

Mishra, Vimal, et al., 2019. Drought and famine in India, 1870–2016. Geophys. Res. Lett. 46 (4), 2075–2083.

Monirul Qader Mirza, M., 2005. Vulnerability to the Ganges water diversion: adaptation and coping mechanisms. In: The Ganges Water Diversion: Environmental Effects and Implications. Springer, pp. 247–285.

Monteith, John L., 1965. Evaporation and environment. In: Symposia of the Society for Experimental Biology. Vol. 19, Cambridge University Press (CUP) Cambridge, pp. 205–234.

Moraes, O, et al., 2021. The 2019–2021 extreme drought episode in La Plata Basin.

Morales, Mariano S, et al., 2020. Six hundred years of South American tree rings reveal an increase in severe hydroclimatic events since mid-20th century. Proc. Natl. Acad. Sci. 117 (29), 16816–16823.

Mukherjee, Sourav, Mishra, Ashok, Trenberth, Kevin E., 2018. Climate change and drought: a perspective on drought indices. Curr. Clim. Chang. Rep. 4, 145–163.

Naumann, Gustavo, et al., 2023. Extreme and long-term drought in the La Plata Basin: event evolution and impact assessment until September 2022.

Nguyen, Phuong-Loan, Min, Seung-Ki, Kim, Yeon-Hee, 2021. Combined impacts of the El Niño-Southern Oscillation and Pacific decadal oscillation on global droughts assessed using the standardized precipitation evapotranspiration index. Int. J. Climatol. 41, E1645–E1662.

Otto, Friederike EL, et al., 2018. Anthropogenic influence on the drivers of the Western Cape drought 2015–2017. Environ. Res. Lett. 13 (12), 124010.

Parry, Simon, et al., 2012. Multi-year droughts in Europe: analysis of development and causes. Hydrol. Res. 43 (5), 689–706.

Pascale, Salvatore, et al., 2020. Increasing risk of another Cape Town "Day Zero" drought in the 21st century. Proc. Natl. Acad. Sci. 117 (47), 29495–29503.

Pascale, Salvatore, et al., 2021. Natural variability vs forced signal in the 2015–2019 Central American drought. Clim. Change 168, 1–21.

Penman, Howard Latimer, 1948. Natural evaporation from open water, bare soil and grass. Proc. R. Soc. Lond. Ser. A. Math. Phys. Sci. 193 (1032), 120–145.

Perry, A.H., 1976. The long drought of 1975–76. Weather 31 (10), 328–336.

Rakovec, Oldrich, et al., 2022. The 2018–2020 multi-year drought sets a new benchmark in Europe. Earth's Futur. 10 (3), e2021EF002394.

Reddy, P Jyoteeshkumar, et al., 2022. Combined role of ENSO and IOD on compound drought and heatwaves in Australia using two CMIP6 large ensembles. Weather. Clim. Extrem. 37, 100469.

Richman, Michael B., Leslie, Lance M., 2015. Uniqueness and causes of the California drought. Procedia Comput. Sci. 61, 428–435.

Rivera, Juan A., 2024. Characterization of the recent (2019–2022) La Plata Basin hydrological drought from a centennial-scale perspective. HydroResearch.

Rivera, Juan A, et al., 2021. A decade of hydrological drought in Central-Western Argentina. Front. Water 3, 640544.

Ruijsch, Denise, et al., 2024. Thrive or wither: Exploring the impacts of multi-year droughts on vegetation. Authorea Prepr..

Sgroi, Leandro Carlos, et al., 2021. Characteristics of droughts in Argentina's core crop region. Hydrol. Earth Syst. Sci. 25 (5), 2475–2490.

Singh, V.P., Guo, H., Yu, F.X., 1993. Parameter estimation for 3-parameter log-logistic distribution (LLD3) by Pome. Stoch. Hydrol. Hydraul. 7, 163–177.

Sinha, Ashish, et al., 2011. A global context for megadroughts in monsoon Asia during the past millennium. Quat. Sci. Rev. 30 (1–2), 47–62.

Spinoni, Jonathan, et al., 2019. A new global database of meteorological drought events from 1951 to 2016. J. Hydrol.: Reg. Stud. 22, 100593.

Thornthwaite, Charles Warren, 1948. An approach toward a rational classification of climate. Geogr. Rev. 38 (1), 55–94.

Um, Myoung-Jin, et al., 2017. Effects of different reference periods on drought index (SPEI) estimations from 1901 to 2014. Hydrol. Earth Syst. Sci. 21 (10), 4989–5007.

Ummenhofer, Caroline C, et al., 2009. What causes southeast Australia's worst droughts? Geophys. Res. Lett. 36 (4).

University of East Anglia Climatic Research Unit Jones, P.D., Harris, I.C., 2008. Climatic Research Unit (Cru): Time-Series (TS) Datasets of Variations in Climate with Variations in Other Phenomena V3. NCAS British Atmospheric Data Centre, URL: http://catalogue.ceda.ac.uk/uuid/3f8944800cc48e1cbc29a5ee12d8542d. (Accessed 04 2023).

Van der Wiel, Karin, Batelaan, Thomas J., Wanders, Niko, 2023. Large increases of multi-year droughts in north-western Europe in a warmer climate. Clim. Dyn. 60 (5), 1781–1800.

Van der Wiel, Karin, Lenderink, Geert, de Vries, Hylke, 2021. Physical storylines of future European drought events like 2018 based on ensemble climate modelling. Weather. Clim. Extrem. 33, 100350.

Van Dijk, Albert IJM, et al., 2013. The Millennium Drought in southeast Australia (2001–2009): Natural and human causes and implications for water resources, ecosystems, economy, and society. Water Resour. Res. 49 (2), 1040–1057.

Vicente-Serrano, Sergio M, Beguería, Santiago, López-Moreno, Juan I, 2010. A multi-scalar drought index sensitive to global warming: the standardized precipitation evapotranspiration index. J. Clim. 23 (7), 1696–1718.

Vijverberg, Sem, Coumou, Dim, 2022. The role of the Pacific Decadal Oscillation and ocean-atmosphere interactions in driving US temperature predictability. Npj Clim. Atmos.heric Sci. 5 (1), 18.

Vonk, M.A., 2022. SPEI: A Simple Python Package to Calculate and Visualize Drought Indices (v0.3.5). Zenodo, URL: https://doi.org/10.5281/zenodo.10816741.

Vremec, M., Collenteur, R.A., Birk, S., 2023. Technical note: Improved handling of potential evapotranspiration in hydrological studies with *PyEt*. Hydrol. Earth Syst. Sci. Discuss. 2023, 1–23. http://dx.doi.org/10.5194/hess-2022-417, URL: https://hess.copernicus.org/preprints/hess-2022-417/.

Wu, Guiyang, et al., 2022. Impacts of climate change on global meteorological multi-year droughts using the last millennium simulation as a baseline. J. Hydrol. 610, 127937.

Yevjevich, Vujica M., et al., 1967. An Objective Approach to Definitions and Investigations of Continental Hydrologic Droughts, vol. 23, Colorado State University Fort Collins, CO, USA.

Zotarelli, Lincoln, et al., 2010. Step by step calculation of the Penman-Monteith evapotranspiration (FAO-56 method). Inst. Food Agric. Sci. Univ. Fla. 8.